Results in Physics 59 (2024) 107587

Contents lists available at ScienceDirect

Results in Physics

journal homepage: www.elsevier.com/locate/rinp

# Enhanced performance and stability of quasi two-dimensional perovskite solar cells by conductive phosphine oxide

Chenguang Xia, Yuefeng Liu, Zhenlong Zhang *

*School of Physics and Electronics, Henan University, Kaifeng 475004, China*

ARTICLE INFO

*Keywords:*
Conductive phosphine oxide
Perovskite solar cells
Enhanced efficiency

ABSTRACT

Recently, quasi two-dimensional (quasi-2D) perovskite solar cells (PSCs) have been paid more attentions due to their good stability. While the efficiency of 2D PSCs is lower than that of 3D ones due to their poor charge transport property. Here we introduced a conductive material of 2,7-bis(diphenylphosphoryl)-9,9′-spirobifluorene (SPPO13) into the precursor solution of quasi-2D perovskite $GAMA_5Pb_5I_{16}$ (GA = guanidinium, MA = methylammonium) to improve the charge transfer property. The efficiency of the PSCs with SPPO13 is increased to 18.58 % from 16.97 % for the control, which is resulting from the enlarged grain size, increased electrical conductivity, and reduced trap state density induced by the addition of SPPO13. Moreover, the additon of SPPO13 improves the stability of the devices. The normalized PCE of the devices with SPPO13 keeps 90 % of the original value after aging for 30 days in atmosphere. This study provides a novel way to enhance the charge transfer property of 2D perovskite by conductive material for enhanced efficiency and stability of quasi-2D PSCs.

## Introduction

In the past years, the perovskite solar cells (PSCs) have drawn more attentions due to their intriguing photoelectric properties [1–3]. The power conversion efficiency (PCE) of the PSCs has reached to 26.2 % [4]. However, the instability of three-dimensional (3D) PSCs is a challenge for their industrialization. Recently, quasi two-dimensional (quasi-2D) PSCs have drawn more interests due to their excellent stability [5–7]. Typically, the 2D perovskite contains three types, Ruddlesden-Popper (RP), alternating cations in the interlayer space (ACI), and Dion-Jacobson (DJ) phases. The ACI phase is depicted with an expression of $GAMA_nPb_nI_{3n+1}$ (GA = guanidinium, MA = methylammonium). Compared with RP phase 2D perovskite, ACI phase 2D perovskite has smaller energy bandgap, longer carrier lifetime, and lower exciton binding energy [8,9].

Despite better stability, the efficiencies of the quasi-2D PSCs are still lower than those of 3D ones. The main reason is that charge transport is poor for 2D perovskite because of the insulating property of organic spacers [10]. To solve the issues, some methods have been adopted, such as design of bulky organic cations [11], additive engineering [12], and hot casting [13]. In these methods, additive engineering is an effective and widely used method. Zhang *et al.* [14] added the additive of methylammonium thiocyanate (MASCN) to the 2D perovskite (BDA)$_4Pb_5I_{16}$ to improve the phase distribution, crystalline quality, and carrier transport of perovskite films, thus a high efficiency of 18.72 % was achieved. Luo *et al.* [15] added the MACl additive to the 2D perovskite (GA)$(MA)_3Pb_3I_{10}$ to enhance the charge transport property, thus an efficiency of 18.48 % was obtained. Zheng *et al.* [16] introduced thio-semicarbazide (TSC) additive into the 2D precursor of $(BA)_2(MA)_3Pb_4I_{13}$ to induce uniform morphology, increased grain size and vertical orientation, resulting in a PCE boosting from 1.05 % to 14.15 %. Sun *et al.* [17] applied dual additives of MACl and GuSCN to the 2D perovskite 4F-$PEA_2MA_4Pb_5I_{16}$ to enhance the film quality and crystal orientation and obtained an efficiency of 15.05 % for the planar p-i-n PSCs.

However, most of the additives reported are electrical insulating, which could deteriorate the charge transport of the perovskite, thus reducing the device performance. It is a potential way to incorporate conductive additives into the perovskite to improve the charge transport property for enhancing their efficiency [18,19]. However, there are few reports on the application of conductive additive to the quasi-2D PSCs. The 2,7-bis(diphenylphosphoryl)-9,9′-spirobifluorene (SPPO13) is a conductive material, which has been applied to organic light-emitting diode as an electron transport layer [20], and perovskite light-emitting diode as a perovskite surface passivator [21].

In this work, we introduced the conductive material of SPPO13 into

* Corresponding author.
*E-mail address:* zhenlong2015@163.com (Z. Zhang).

https://doi.org/10.1016/j.rinp.2024.107587
Received 24 November 2023; Received in revised form 6 March 2024; Accepted 17 March 2024
Available online 18 March 2024

the precursor solution of ACI phase perovskite $GAMA_5Pb_5I_{16}$ to improve the charge transfer property of the 2D perovskite. The efficiency of the PSCs with SPPO13 is increased to 18.33 % from 16.77 % for those without additive. Moreover, the addition of SPPO13 improves the the stability of the devices.

## Experimental section

### *Chemicals*

Methylammonium iodide (MAI, 99.5 %), Guanidinium iodide (GAI, 99.5 %), Spiro-OMeTAD (99.8 %), 2,7-bis(diphenylphosphoryl)-9,9′-spirobifluorene (SPPO13, 99 %), methylammonium chloride (MACl, 99.5 %), and lead iodide ($PbI_2$, 99.999 %) were phased from Xi'an p-OLED Company. The $SnO_2$ colloid solution was bought from Alfa Aesar. Dimethylsulfoxide (DMSO, 99.95 %), ethyl acetate (EA, 99.5 %), and N, N-dimethylformamide (DMF, 99.8 %) were obtained from Shanghai Aladdin Technology.

### *Fabrication of PSCs*

The ITO was rinsed in acetone, isopropanol and ethanol for 20 min, respectively. A $SnO_2$ solution (8 %) was spin-coated on the ITO glass substrate (4000 rpm, 30 s), and dried at 150 °C for 30 min to prepare an electron transport layer (ETL). A perovskite absorption layer was prepared on the ETL by spin-coating a perovskite solution (4000 rpm, 25 s), and 150 μl of EA solution was dropped rapidly, then heating for 12 min at 100 °C. The perovskite $GAMA_5Pb_5I_{16}$ precursor solution was obtained by dissolving 414.9 mg $PbI_2$, 168.3 mg GAI, and 143.1 mg MAI, and in 1 ml mixture solvent of DMF and DMSO (4:1, v/v). The perovskite with additive was obtained by putting a certain amount of SPPO13 into the perovskite solution. A hole transport layer (HTL) was prepared by spin-coating Spiro-OMeTAD solution on the perovskite layer (4000 rpm, 30 s). Lastly, an Au electrode with 90 nm thickness was formed on the HTL.

### *Characterization*

The X-ray diffraction (XRD) was obtained by an instrument (Bruker). The X-ray photoelectron spectroscopy (XPS) was obtained on a spectrometer (Thermofisher ESCALAB Xi + ). The steady-state photoluminescence (PL) and time-resolved PL (TRPL) were recorded with a diffractometer (FLS 980, England). The UV–visible absorption was performed with an instrument (Carry 5000). The scanning electron microscope (SEM) was measured with an apparatus (JSM-7001F). The electrochemical impedance spectra (EIS) were conducted by an electrochemical workstation (CHI660e). The atom force microscope (AFM) was recorded by an apparatus (NT-MDT Solver P47H-PRO). The J-V plots were obtained with a Keithley 2400 source meter with a solar light simulator.

## Results and discussion

The molecular structure of SPPO13 is displayed in Fig. 1a, which contains two phosphine oxide functional groups. In this study, the PSCs

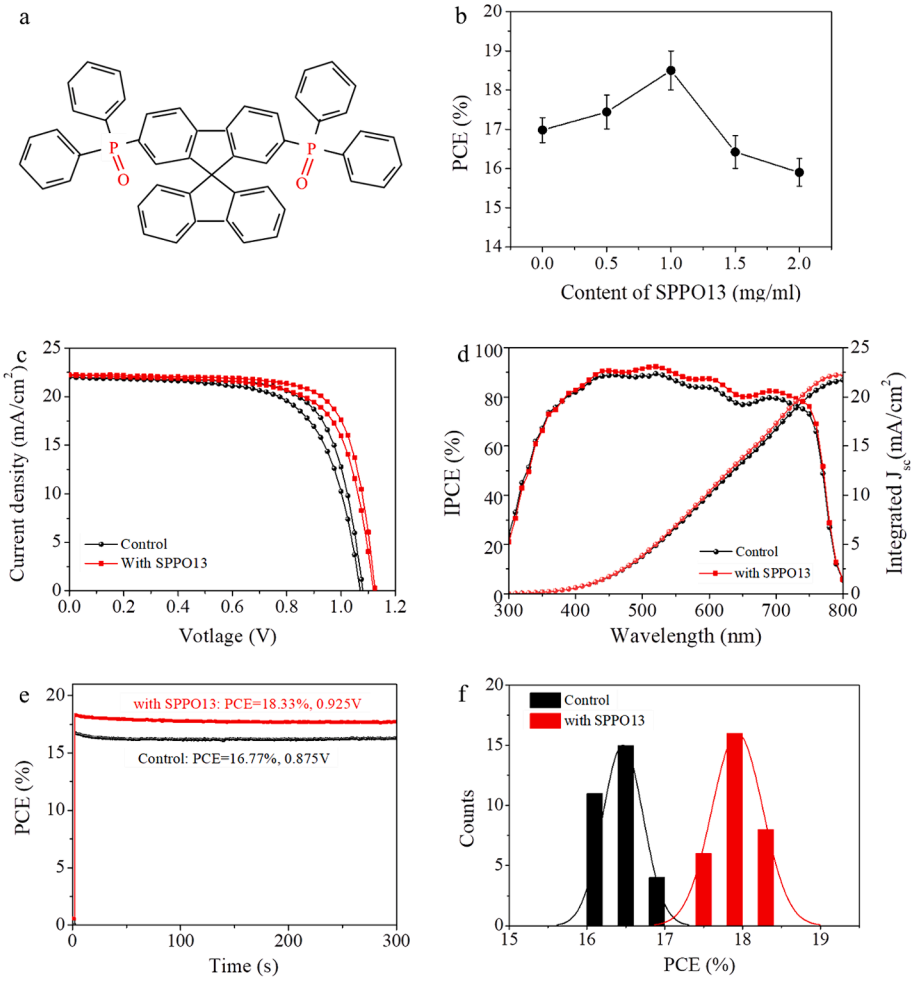


**Fig. 1.** (a) Molecular structure of SPPO13. (b) Relationship between PCE of the solar cells and content of SPPO13. (c) J-V curves, (d) IPCE, and (d) Steady-state output of the champion PSCs. (e) PCE distribution.

with a configuration of ITO/$SnO_2$/$GAMA_5Pb_5I_{16}$ (SPPO13)/Spiro-OMeTAD/Au were prepared, in which the perovskite layer is the 2D ACI phase perovskite $GAMA_5Pb_5I_{16}$ with additive SPPO13. We also fabricated the PSCs without additive for comparison, which is referred as the control. An important element to affect the performance of the PSCs is the content of additive, thus the content of SPPO13 was optimized. Fig. 1b presents the relationship between PCE of the PSCs and the content of SPPO13. It can be seen that the efficiency of the PSCs is the maximum at the content of 1 mg/mL. Thereinafter the optimized SPPO13 content of 1 mg/mL was used to fabricate the PSCs.

Table 1 provides the statistical performance parameters of the PSCs with and without SPPO13 calculated from 20 devices. The mean value of PCE for the devices with SPPO13 is improved to 17.93 % from 16.46 % for those without additive. Fig. 1c shows the J-V curves with forward scan (FS) and reverse scan (RS) of the champion solar cells with and without SPPO13, and their performance parameters are tabulated in Table 2. The short circuit current ($J_{sc}$) of the solar cell with SPPO13 is nearly same to the control. While the open circuit voltage ($V_{oc}$) of the solar cell with SPPO13 is increased to 1.125 V (RS) from 1.079 V for the control. This suggests that the PCE improvement is mainly attributed to the $V_{oc}$ increase. A high efficiency of 18.58 % is obtained for the device with SPPO13 at the RS direction, while that of the device without additive is 16.97 %. In addition, Hysteresis index (HI) was calculated by the equation [22],

$$HI = \frac{PCE_{RS}\text{-}PCE_{FS}}{PCE_{RS}} \quad (1)$$

where $PCE_{RS}$ and $PCE_{FS}$ are the efficiency at the direction of reverse scan and forward scan, respectively. The HI value of the device with SPPO13 is 0.057, which is smaller than that of the control (0.070), which suggests that the addition of SPPO13 significantly decreases the HI of the solar cells. Fig. 1d displays the IPCE spectra of the PSCs. The integrated short circuit current density ($J_{sc}$) was calculated to be 22.22 mA/cm$^2$ for the PSCs with SPPO13, which is larger than that of the control (21.75 mA/cm$^2$). Fig. 1e provides the stabilized power output measured at a maximum power point. The stead state PCE of the solar cell increases to 18.33 % from 16.77 % with the addition of SPPO13, which agrees well with those obtained from J-V measurements. Fig. 1f presents the PCE distribution for the PSCs with and without SPPO13. Both the perovskite solar cells present good reproducibility.

To check the effect of additive on the morphology of the perovskite (PVK), we carried out SEM measurements. Fig. 2a and b show the SEM of the PVK films with and without SPPO13. The perovskite film without SPPO13 contains some small grains, which overlap each other and distribute loosely. While the grain size of the PVK film with SPPO13 becomes large, and the perovskite film are compact and flat. We further performed AFM measurements to explore the effect of the additive on the PVK surface roughness. Fig. 2c and d show the AFM pictures of the PVK films without and with SPPO13. The root mean square (RMS) of the PVK film with SPPO13 decreases to 17.1 nm from 24.2 nm for that without additive, which suggests that the addition of SPPO13 makes the perovskite film smoother. It is beneficial to the contact between the HTL and PVK layer, favoring carrier extraction and transport [23].

The crystallinity of the perovskite was investigated by XRD. Fig. 3a provides the XRD of the PVK films without and with SPPO13. The peaks standed on 28.27° and 14.07°could be attributed to (220) and (110) crystal planes of the perovskite $MAPbI_3$, respectively [24,25]. The peak intensity of the PVK film becomes stronger with the addition of SPPO13,

**Table 1**
Statistical photovoltaic parameters of the PSCs obtained from 20 devices.

| Device | $J_{sc}$ (mA/cm$^2$) | $V_{oc}$ (V) | FF (%) | PCE (%) |
|---|---|---|---|---|
| Control | 21.96 ± 0.28 | 1.071 ± 0.022 | 70.1 ± 0.12 | 16.46 ± 0.59 |
| with SPPO13 | 22.29 ± 0.26 | 1.116 ± 0.016 | 72.0 ± 0.09 | 17.93 ± 0.57 |

**Table 2**
Performance parameters of the champion PSCs.

| Device | Scan | $J_{sc}$ (mA/cm$^2$) | $V_{oc}$ (V) | FF (%) | PCE (%) | HI |
|---|---|---|---|---|---|---|
| Control | FS | 22.01 | 1.069 | 67.1 | 15.79 | 0.070 |
| | RS | 22.01 | 1.079 | 71.5 | 16.97 | |
| with SPPO13 | FS | 22.23 | 1.121 | 70.4 | 17.53 | 0.057 |
| | RS | 22.23 | 1.125 | 74.3 | 18.58 | |

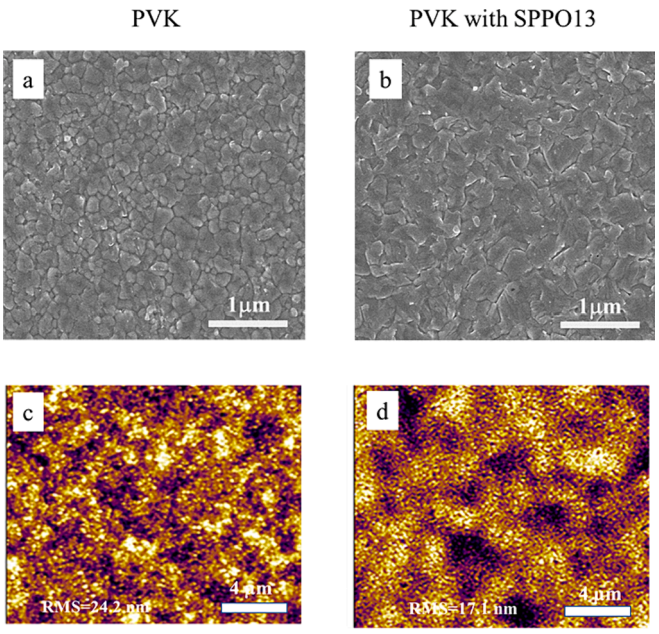


**Fig. 2.** SEM and AFM of the PVK films without and with SPPO13.

which indicates that the addition of SPPO13 improves the crystallinity of the perovskite. The full width at half maximum (FWHM) of the strongest peak (110) of the PVK with SPPO13 is decreased to 0.273° compared with that of the pristine (0.313°), which suggests a better crystallinity of the perovskite with addition of SPPO13. Fig. 3b displays the magnified XRD patterns at the range of 5°~12°. The peaks at 8.20° and 9.92° could correspond to n = 3 and other lower n-value phases of 2D perovskite $GAMA_nPb_nI_{3n+1}$ [26,27]. These results demonstrate that the prepared perovskite of $GAMA_5Pb_5I_{16}$ is a hybrid film which contains dominated 3D phase $MAPbI_3$ and some low-dimensional 2D phases. To investigate the interaction between SPPO13 and perovskite, we recorded XPS of the PVK with and without SPPO13 as shown in Fig. 3c. With the addition of SPPO13, the characteristic peaks of Pb $4f_{7/2}$ and Pb $4f_{5/2}$ move to lower binding energy 137.7 and 142.6 eV from 138.2 and 143.1 eV, respectively. This could be attributed to the changes in electron cloud density of $Pb^{2+}$ [21].

To explore the effect of SPPO13 on the optical property of the PVK film, UV–vis absorption of the perovskite were measured and presented in Fig. 4a. Both of them are similar with an absorption onset wavelength at about 780 nm [25]. We carried out PL and TRPL measurements to investigate the effect of SPPO13 on the trap state density. Fig. 4b presents the stead state PL spectra of the PVK films with and without SPPO13. A PL peak located at about 774 nm is observed, which is in accordance to the previous report [25]. The PVK film with SPPO13 exhibits an enhanced PL intensity compared with the PVK film without SPPO13, which suggests that the addition of SPPO13 is favorable to reduce the trap state density of the PVK. Moreover, we measured the TRPL of the PVK films as shown in Fig. 4c. The TRPL was analyzed by a biexponential equation [28,29],

$$I(t) = A_1\exp_1^{(-t/\tau)} + A_2\exp_2^{(-t/\tau)} \quad (2)$$

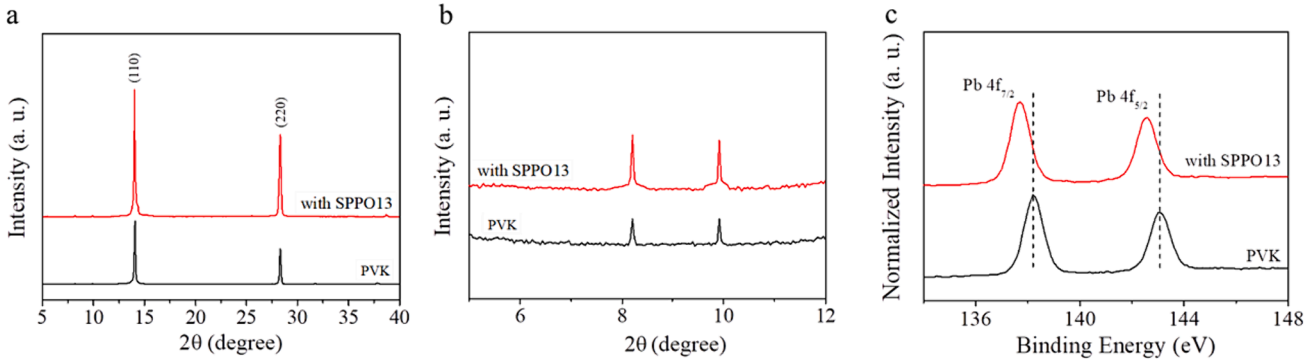


**Fig. 3.** (a) XRD, (b) Magnified XRD at the range of 5°~12°, and (c) XPS of the perovskite films without and with SPPO13.

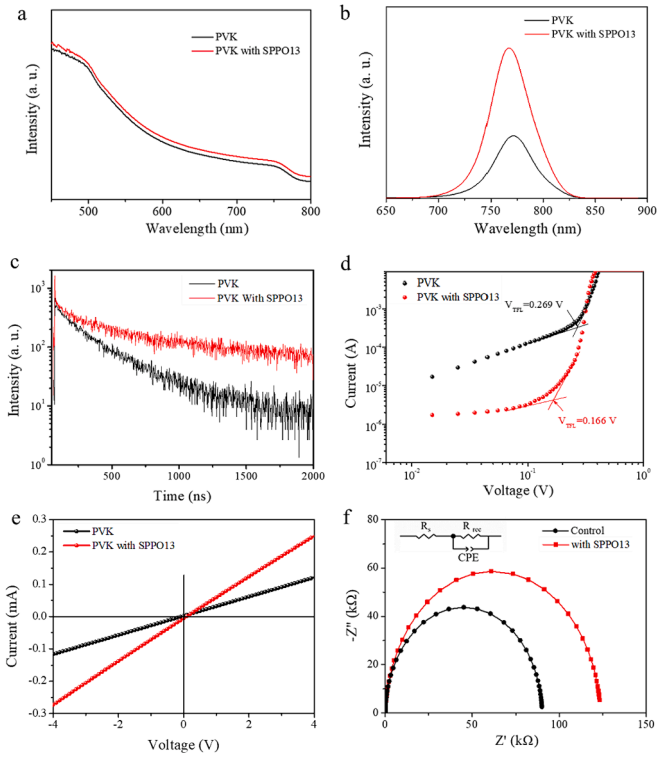


**Fig. 4.** (a) UV–vis absorption, (b) PL, and (c) TRPL of the PVK films without and with SPPO13. (d) J-V curves of electron-only devices with a configuration of ITO/$SnO_2$/PVK (PVK with SPPO13)/PCBM/Au. (e) I-V plots recorded from the devices with a structure of ITO/PVK (PVK with SPPO13) /Au. (f) Nyquist plots.

where $\tau_1$ is a fast component associated with non-radiative recombination due to the defects. $\tau_2$ is a slow component associated with radiative recombination. The average lifetime ($\tau_{ave}$) was calculated by the equation [30],

$$\tau_{ave} = \frac{\sum A_i \tau_i^2}{\sum A_i \tau_i} \quad (3)$$

Table 3 lists the obtained parameters by fitting the TRPL. The $\tau_{ave}$ of the perovskite film with SPPO13 is 491.9 ns, which is larger than that without additive (304.8 ns). This proves that the addition of SPPO13 induces the defects of the PVK film decreased [31]. To further get an insight into the effect of SPPO13 on the trap states, space-charge-limited current (SCLC) was performed. Fig. 4d provides the dark J-V measurements of electron-only device with a configuration of ITO/$SnO_2$/PVK (PVK with SPPO13)/PCBM/Au. The trap state density ($N_t$) of PVK film can be calculated with the formula [32,33],

$$N_t = 2\varepsilon_0\varepsilon_r V_{TFL}/(qL^2) \quad (4)$$

where $\varepsilon_0$ stands for the vacuum permittivity of the PVK, and $\varepsilon_r$ is the relative permittivity of the PVK. L is the length between ITO and Au, and q is the elementary charge. $V_{TFL}$ is the trap-filled limit (TFL) voltage. The $N_t$ of the PVK film with SPPO13 was calculated to be $1.64 \times 10^{15}$ $cm^{-3}$, which is less than that of the PVK film without additive ($2.65 \times 10^{15}$ $cm^{-3}$). This suggests that the addition of SPPO13 reuslts in reduced trap states of the PVK film, which agrees well with the results from the PL and TRPL measurements. The reduced trap state density and carrier recombination of the perovskite films with SPPO13 could contribute the increased $V_{oc}$ of the solar cells.

To investigate the effect of SPPO13 on the electrical conductivity of the perovskite film, I-V spots of the devices with a configuration of ITO/PVK (PVK with SPPO13)/Au were recorded and provided in Fig. 4e. According to the equation [34,35], $\sigma_2/\sigma_1 = I_2/I_1$, the calculated electrical conductivity of the perovskite film with SPPO13 is enhanced by 2.1 times than that without additive. This is conducive to the charge transport for the 2D perovskite. We further applied electrochemical impedance spectra (EIS) to check the charge transfer behavior in the PSCs [36]. Fig. 4f provides the Nyquist plots of the devices, which can be analyzed by an equivalent circuit in Fig. 4f, where $R_s$, CPE and $R_{rec}$ represent a series resistance, a constant phase element and a recombination resistance [37]. The obtained parameters are presented in Table 4. The recombination resistance $R_{rec}$ of the device with SPPO13 is 123570 Ω·$cm^2$, which is much larger than that of the control (90046 Ω·$cm^2$). This suggests that the addition of SPPO13 is conducive to the reduction of the interfacial carrier recombination.

Based on the above analysis, we conclude that the performance enhancement of the PSCs with SPPO13 is manily attributed to the enlarged grain size, increased electrical conductivity, and reduced trap state density induced by the addition of SPPO13.

Stability is a key factor for the industrialization of the PSCs. The effect of SPPO13 addition on the stability of PSCs was investigated.

**Table 3**
Parameters obtained by analyzing the TRPL.

| Sample | $\tau_1$ (ns) | $\tau_2$ (ns) | $B_1$ (%) | $B_2$ (%) | $\tau_{ave}$ (ns) |
|---|---|---|---|---|---|
| PVK | 117.60 | 376.80 | 210.98 | 171.34 | 304.8 |
| with SPPO13 | 58.98 | 541.20 | 100.06 | 95.86 | 491.9 |

**Table 4**
Calculated parameters from the EIS data.

| Device | $R_s$ (Ω·$cm^2$) | $R_{rec}$ (Ω·$cm^2$) | CPE (F/$cm^2$) |
|---|---|---|---|
| Control | 55.08 | 90,046 | 1.135E-8 |
| with SPPO13 | 73.91 | 123,570 | 1.521E-8 |

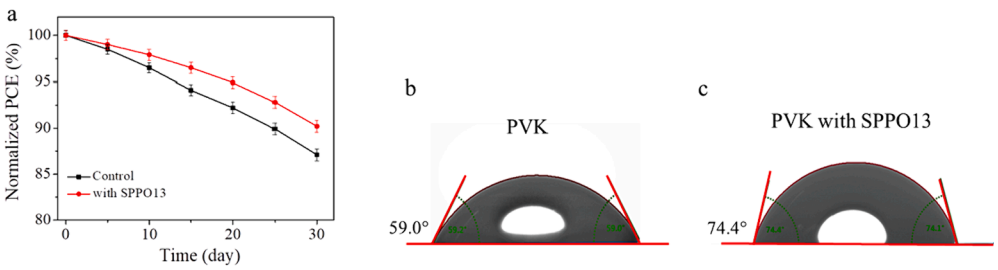


**Fig. 5.** (a) Dependence of normalized PCE on the aging time in atmosphere (25 °C, RH 30 %). WCA of the PVK films (b) without, and (c) with SPPO13.

Fig. 5a shows the dependence of normalized PCE on aging time in atmosphere (25 °C, RH 30 %). The solar cells with SPPO13 maintain 90 % of the original PCE after 30 days, while the devices without additive maintain 87 % of the original PCE. This demonstrates that the addtion of SPPO13 enhances the stability of the PSCs. To investigate the stability improvement, we measured the water contact angles (WCA) of the PVK films and provided in Fig. 5b and c. The WCA value of the PVK film with SPPO13 increases to 74.4° from 59.0° for that without additive. This indicates that a better hydrophobicity of the PVK film is obtained by the addition of SPPO13. The better hydrophobicity of the perovskite films with SPPO13 can prevent the water molecules permeating into the perovskite to make it decompose, thus enhancing the stability of the solar cells. The hydrophobicity improvement could be originated from the improved morphology and film quality [38].

## Conclusion

In this work, we added the conductive material of SPPO13 into the precursor solution of 2D ACI phase perovskite $GAMA_5Pb_5I_{16}$. The addition of SPPO13 leads to enlarged grain size, increased electrical conductivity, and reduced trap state density, thus the PCE of the PSCs with SPPO13 is increased to 18.58 % from 16.97 % for the control devices. In addition, the stability of the PSCs is enhanced. The PCE of the devices with SPPO13 maintain 90 % of the original after 30 days in atmosphere. This work is significant to improve the charge transfer property of 2D perovskite and enhance the efficiency and stability of quasi-2D PSCs.

## CRediT authorship contribution statement

**Chenguang Xia:** Investigation. **Yuefeng Liu:** Methodology. **Zhenlong Zhang:** Writing – review & editing, Conceptualization.

## Declaration of competing interest

The authors declare that they have no known competing financial interests or personal relationships that could have appeared to influence the work reported in this paper.

## Data availability

No data was used for the research described in the article.

## Acknowledgements

The work was supported by the Project of Henan Province Universities (22A140016).

## References

[1] Burschka J, Pellet N, Moon SJ, et al. Sequential deposition as a route to high-performance perovskite-sensitized solar cells. Nature 2013;499:316–9.
[2] Shi D, Adinolfi V, Comin R, et al. Low trap-state density and long carrier diffusion in organolead trihalide perovskite single crystals. Science 2015;347:519–22.
[3] Blancon JC, Blancon J, Stoumpos CC, et al. Semiconductor physics of organic-inorganic 2D halide perovskites. Nat Nanotechnol 2020;15:969–85.
[4] Best Research-Cell Efficiency Chart (NREL, Dec. 10th, 2023), https://www.nrel.gov/pv/cell-efficiency.html.
[5] Lai H, Lu D, Xu Z, et al. Organic-salt-assisted crystal growth and orientation of quasi-2D ruddlesden-popper perovskites for solar cells with efficiency over 19%. Adv Mater 2020;32:2001470.
[6] Liu P, Han N, Wang W, et al. High-quality ruddlesden-popper perovskite film formation for high-performance perovskite solar cells. Adv Mater 2021;33:2002582.
[7] Liang C, Gu H, Xia Y, et al. Two-dimensional ruddlesden-popper layered perovskite solar cells based on phase-pure thin films. Nat Energy 2021;6:38–45.
[8] Zou W, Li R, Zhang S, et al. Minimising efficiency roll-off in high-brightness perovskite light-emitting diodes. Nat Commun 2018;9:608.
[9] Zhang Q, Chu L, Zhou F, et al. Excitonic properties of chemically synthesized 2D organic-inorganic hybrid perovskite nanosheets. Adv Mater 2018;30:1704055.
[10] Yan LF, Ma JJ, Li PW, et al. Charge-carrier transport in quasi-2D ruddlesden-popper perovskite solar cells. Adv Mater 2022;34:2106822.
[11] He T, Li S, Jiang Y, et al. Reduced-dimensional perovskite photovoltaics with homogeneous energy landscape. Nat Commun 2020;11:1–11.
[12] Zhang X, Wu G, Fu W, et al. Orientation regulation of phenylethylammonium cation based 2D perovskite solar cell with efficiency higher than 11%. Adv Energy Mater 2018;8:1702498.
[13] Tsai H, Nie W, Blancon JC, et al. High-efficiency two-dimensional ruddlesden-popper perovskite solar cells. Nature 2016;536:312–6.
[14] Zhang W, Wu X, Zhou J, et al. Pseudohalide-assisted growth of oriented large grains for high-performance and stable 2D perovskite solar cells. ACS Energy Lett 2022;7:1842–9.
[15] Luo T, Zhang Y, Xu Z, et al. Compositional control in 2D perovskites with alternating cations in the interlayer space for photovoltaics with efficiency over 18%. Adv Mater 2019;31:1903848.
[16] Zheng H, Liu D, Wang Y, et al. Synergistic effect of additives on 2D perovskite film towards efficient and stable solar cell. Chem Eng J 2020;389:124266.
[17] Sun LJ, Cao XH, Wang JJ, et al. Synergistic effect of dual anions for efficient and stable quasi 2D perovskite solar cell. J Alloy Compd 2022;918:165725.
[18] Girish KH, Vishnumurthy KA, Roopa TS. Role of conducting polymers in enhancing the stability and performance of perovskite solar cells: a brief review. Mater Today Sustain 2022;17:100090.
[19] Isakova A, Topham PD. Polymer strategies in perovskite solar cells. J Polym Sci B 2017;55:549–68.
[20] Yang LS, Meng HF, Chang YF, et al. Stable and efficient blue fluorescent organic light-emitting diode by blade coating with or without electron-transport layer. Org Electron 2017;51:6–15.
[21] Li ML, Zhao YP, Qin XQ, et al. Conductive phosphine oxide passivator enables efficient perovskite light-emitting diodes. Nano Lett 2022;22:2490–6.
[22] Habisreutinger SN, Noel NK, Snaith HJ. Hysteresis index: a figure without merit for quantifying hysteresis in perovskite solar cells. ACS Energy Lett 2018;3:2472–6.
[23] Yu Z, Zhang L, Tian S, et al. Hot-substrate deposition of hole-and electron-transport layers for enhanced performance in perovskite solar cells. Adv Energy Mater 2018;8:1701659.
[24] Yang J, Yang T, Liu D, et al. Stable 2D alternating cation perovskite solar cells with power conversion efficiency >19% via solvent engineering. Solar RRL 2021;5:2100286.
[25] Zhang ZL, Park NG. Quasi-two-dimensional perovskite solar cells with efficiency exceeding 22%. ACS Energy Lett 2022;7:757–65.
[26] Gu H, Liang C, Xia Y, et al. Nanoscale hybrid multidimensional perovskites with alternating cations for high performance photovoltaic. Nano Energy 2019;65:104050.
[27] Soe CM, Stoumpos CC, Kepenekian M, et al. New type of 2D perovskites with alternating cations in the interlayer space, (C(NH2)3)-(CH3NH3)NPbNI3n+1: structure, properties, and photovoltaic performance. J Am Chem Soc 2017;139:16297–309.
[28] Cai Y, Cui J, Chen M, et al. Multifunctional enhancement for highly stable and efficient perovskite solar cells. Adv Funct Mater 2020;31:2005776.
[29] Zhang Y, Wen J, Xu Z, et al. Effective phase-alignment for 2D halide perovskites incorporating symmetric diammonium ion for photovoltaics. Adv Sci 2021;8:2001433.
[30] Zhang H, Cheng J, Lin F, et al. Pinhole-free and surface-nanostructured NiOx film by room-temperature solution process for high-performance flexible perovskite solar cells with good stability and reproducibility. ACS Nano 2016;10:1503–11.

[31] Bai S, Da P, Li C, et al. Planar perovskite solar cells with long-term stability using ionic liquid additives. Nature 2019;571:245–50.
[32] Bube RH. Trap density determination by space-charge-limited currents. J Appl Phys 1962;33:1733–7.
[33] Brivio F, Walker AB, Walsh A. Structural and electronic properties of hybrid perovskites for high-efficiency thin-film photovoltaics from first-principles. APL Mater 2013;1:042111.
[34] Chen Y, Yin J, Wei Q, et al. Multiple exciton generation in tin-lead halide perovskite nanocrystals for photocurrent quantum efficiency enhancement. Nat Photon 2022;16:485.
[35] Wu W, Wang Q, Fang Y, et al. Molecular doping enabled scalable blading of efficient hole-transport-layer-free perovskite solar cells. Nat Commun 2018;9:1625.
[36] Xu X, Zhang H, Shi J, et al. Highly efficient planar perovskite solar cells with a $TiO_2$/ZnO electron transport bilayer. J Mater Chem A 2015;3:19288–93.
[37] Ren YK, Ding XH, Wu YH, et al. Temperature-assisted rapid nucleation: a facile method to optimize the film morphology for perovskite solar cells. J Mater Chem A 2017;5:20327–33.
[38] Liu YF, Wu ZL, Dou YX, et al. Formamidinium-based perovskite solar cells with enhanced moisture stability and performance via confined pressure annealing. J Phys Chem C 2020;124:12249–58.